Geochemical Perspectives Letters

Sulfur solubility in a deep magma ocean and implications for the deep sulfur cycle

E.S. Steenstra[1,2*], O.T. Lord[3], S. Vitale[1], E.S. Bullock[1], S. Klemme[2], M. Walter[1]

https://doi.org/10.7185/geochemlet.2219

Abstract

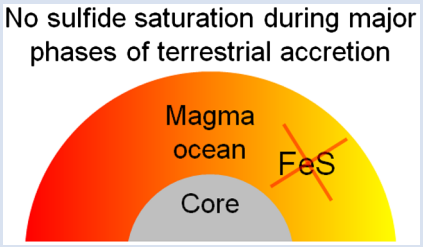

The Earth could have experienced sulfide segregation during its differentiation due to sulfur (S) saturation within a magma ocean. The relative timing of sulfide saturation during magma ocean crystallisation is strongly dependent on the solubility of S at sulfide saturation (SCSS). Here, we present SCSS data directly relevant for a deep terrestrial magma ocean obtained from laser heated diamond anvil cell experiments. Our new data, along with existing SCSS data obtained for similar compositions, was parameterised to derive a new predictive equation. Our parameterisation predicts that existing models strongly underestimate the SCSS over the *P-T* range of a deep magma ocean. Our SCSS models provide the S abundances required at any given stage of terrestrial accretion, and imply that sulfide saturation is much less efficient at stripping the Earth's mantle of S during accretion than previously predicted. Applying our results to the most recent mantle S evolution models shows that the SCSS would be far too high to achieve sulfide saturation, until only perhaps the final stages of magma ocean crystallisation. To satisfy highly siderophile element systematics, either the S content of the magma ocean was considerably higher than currently assumed, or highly siderophile element abundances were affected by other processes, such as iron disproportionation.

Received 5 October 2021 | Accepted 13 April 2022 | Published 20 May 2022

Introduction

Sulfur (S) plays a key role in planetary geochemistry because of its ability to act as a major sink for elements when S is present as a sulfide (Kiseeva and Wood, 2015). Whether sulfide liquid precipitates from a silicate, magma is controlled by the S content at sulfide saturation (SCSS) of that magma. The SCSS is a function of composition, most notably FeO, pressure (*P*) and temperature (*T*), and has been extensively studied at lower pressures (<24 GPa; O'Neill and Mavrogenes, 2002; Namur *et al.*, 2016; Smythe *et al.*, 2017; Ding *et al.*, 2018; Steenstra *et al.*, 2020a,b; Blanchard *et al.*, 2021).

Experimental investigation of metal-silicate partitioning of S during core formation in the Earth suggests mildly siderophile behaviour of S ($D_S^{met-sil}$ = 10–55; Boujibar *et al.*, 2014; Suer *et al.*, 2017). Depending on the core formation scenario, considered S abundances may therefore have been relatively high after core segregation in the magma ocean (Rubie *et al.*, 2016). It has been hypothesised that at some stage the S content of the magma ocean reached the SCSS, due to the incompatible behaviour of S (Callegaro *et al.*, 2020) and the strongly negative dependence of the SCSS on temperature, resulting in segregation of sulfide matte (''the Hadean matte''; O'Neill, 1991). Due to the importance of the Hadean matte for the deep S cycle and chalcophile element abundances, constraints on the SCSS and relative timing of sulfide segregation (during magma ocean crystallisation) are required. Currently, there are no SCSS measurements available at the *P-T* conditions that are directly relevant for a deep(er) magma ocean (>25 GPa; Huang *et al.*, 2020), requiring significant extrapolations of lower pressure data. In addition, the sulfide liquids of many available higher-pressure datasets contain high (>5–15 %) amounts of other elements in addition to Fe-S-O, which will decrease the SCSS (Smythe *et al.*, 2017).

To determine the SCSS in a deep terrestrial magma ocean, FeS-rich sulfide liquids and silicate MORB melts were equilibrated in 3 experiments at 43–53 GPa and 3925–4600 K by laser heating in a diamond anvil cell at the University of Bristol, UK (Table 1). A MORB composition was chosen to ensure that the silicate melt could be quenched to a glass. Run products were analysed using a JEOL JXA 8530F field emission electron microprobe at the Carnegie Institution for Science, USA. The reader is referred to the Supplementary Information file for additional details on experimental and analytical techniques.

Results

The heated spots of the run products were characterised by homogeneous quenched silicate melts with abundant submicron quenched FeS droplets (Fig. 1; Supplementary Information). Sulfur contents of the silicate melts varied between 0.70 and 1.18 wt. % (Fig. 2) and FeO contents significantly

1. Earth and Planets Laboratory, Carnegie Institution of Science, Washington DC, USA
2. Institute of Mineralogy, University of Münster, Germany
3. School of Earth Sciences, University of Bristol, UK
* Corresponding author (email: esteenst@uni-muenster.de)

Table 1 Experimental run conditions and results.

Experiment	P(GPa)[a]	P(GPa)[c]	T(K)	log FeO	SCSS (ppm)
ESS-DAC-4	40 ± 2[b]	53 ± 2[b]	4605 ± 117	1.08(1)	6979 ± 350
ESS-DAC-5	35 ± 2	43 ± 2	4300 ± 129	1.26(1)	10837 ± 2124
ESS-DAC-7	38 ± 2	44 ± 2	3927 ± 37	1.42(1)	11806 ± 780

[a] Defined as the average of the pre- and post-heating measured pressures. [b] Pressure uncertainties are based on Walter *et al.* (2015). [c] Post-heating pressures corrected upwards for thermal pressure effects and subsequently used in this study (Supplementary Information).

increased relative to the starting composition, consistent with previous studies on basaltic melts (Blanchard *et al.*, 2017; Suer *et al.*, 2021). This is likely a result of small differences in the ratio of FeS to silicate within the heated region and variable degrees of perovskite crystallisation on the edges of the heated spot. The data reproduce a positive dependency between FeO content and the SCSS as thermodynamically and experimentally predicted from low *P-T* experiments (Wykes *et al.*, 2015), strongly suggesting sulfide saturation of the melts at high *P-T* (Supplementary Information, Fig. 2a). After normalisation of the SCSS to a common FeO content ($x_{FeO}^{sil\ melt} = 0.05$ or 8.1 wt. % FeO, corresponding to the present day terrestrial primitive mantle; Palme and O'Neill, 2014) using the FeO term of an existing SCSS model (Supplementary Information, section S.3), the effects of *P-T* on the SCSS at the conditions of a deep magma ocean are assessed (Fig. 2c–d). Our results confirm the increase of the SCSS with increasing *T* and the decrease of the SCSS with *P* (O'Neill and Mavrogenes, 2002; Blanchard *et al.*, 2021), as seen in previous low *P-T* data (Ding *et al.*, 2018; Steenstra *et al.*, 2018). Our FeO-normalised SCSS values are consistently higher than predicted by existing high-*P* peridotite models (Laurenz *et al.*, 2016; Blanchard *et al.*, 2021), with an offset of up to +6700 ppm (Fig. 2b). The differences between our FeO-normalised SCSS values and modelled SCSS values are significantly larger when implementing the other published SCSS models. These models are based on a wide range of silicate compositions and, when calculated using raw FeO contents, the differences between our measured and calculated SCSS values are at least 5000 ppm and as high as 1.07 wt. % (Fig. 2b). This shows that the models are not reliable at the conditions of a deep magma ocean. However, because previous parameterisations (Laurenz *et al.*, 2016; Blanchard *et al.*, 2021) were derived for a peridotitic melt, an assessment of the potential effects of non-FeO silicate melt variation on the SCSS is required. Using the Smythe *et al.* (2017) model at 1873 K and 1 GPa, calculated SCSS values for a peridotitic melt (Palme and O'Neill, 2014) are ≈860–1250 ppm higher than for our experimental silicate melt compositions for 8.1 wt. % FeO. A higher SCSS calculated for peridotite is also generally consistent with the results of Laurenz *et al.* (2016). The large offset of our measured SCSS values compared to predicted values confirms that either the positive *T* effects on SCSS were underestimated and/or negative *P* effects were overestimated in previous SCSS models.

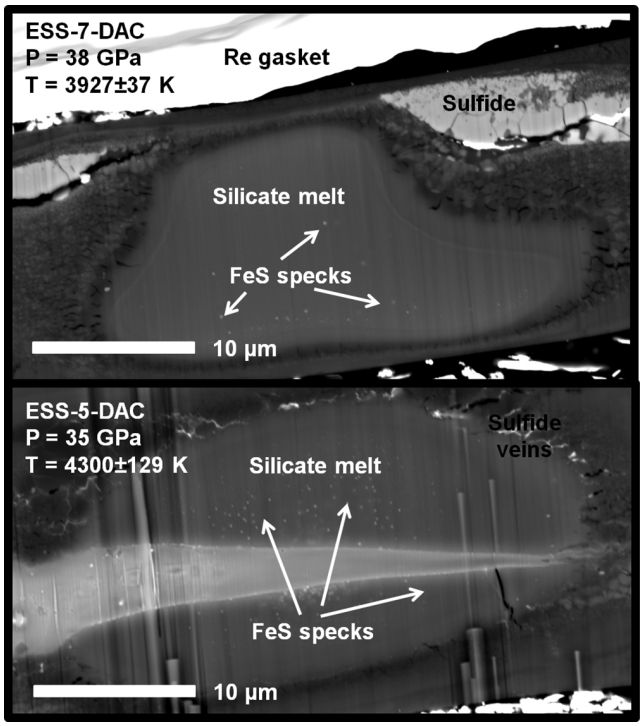

Figure 1 Backscattered electron images of runs ESS-5-DAC and ESS-7-DAC. Line in ESS-5-DAC is a decompression crack.

Discussion

Modelling the solubility of S in a terrestrial magma ocean requires knowledge of the variation of the SCSS with *P-T* (*e.g.*, Boukare *et al.*, 2019). High-*P* data for the SCSS of FeS-rich liquids are relatively scarce in the literature and predominantly derived for peridotite liquids. This prohibits a quantitative assessment of the effects of silicate melt composition at high *P*, which could be very different at such conditions, and constraining this would require tens, if not hundreds, of additional experiments at such conditions. It is also very likely that strong correlations exist between fitted melt composition parameters and *P-T* effects, given that such regressions contain up to 11 terms. Instead, we fitted our new data together with all previous SCSS data that was obtained for very similar compositions (Table S-2; Supplementary Information) to Equation 1:

$$\ln(S)_{SCSS} = a + b\left(\frac{1}{T(K)}\right) + c\left(\frac{P(GPa)}{T(K)}\right) + \ln(a_{FeS}^{sulfide}) \qquad \text{Eq. 1}$$

Prior to fitting, all data were normalised to a common FeO value of 8.1 wt. % ($x_{FeO}^{sil\ melt} = 0.05$) (Supplementary Information, section S.3). The SCSS does not vary significantly (200–300 ppm) within the FeO range relevant for terrestrial magma ocean crystallisation (2 to 8.1 wt. % FeO; Tagawa *et al.*, 2021; Fig. 2a) and no FeO term is required for the parameterisation.

Fitting FeO-normalised literature SCSS data obtained for silicate melts with very similar compositions ($N = 42$; Supplementary Information, section S.5) and assuming $a_{FeS}^{sulfide} = 1$, yields:

$$\ln(S)_{SCSS} = 11.79(62) + \frac{-7073(993)}{T(K)} + \frac{-92(36)*P(GPa)}{T(K)} \times R^2 = 0.86 \qquad \text{Eq. 2}$$

The regression results suggest that the negative pressure effect on the SCSS is (significantly) smaller than previously

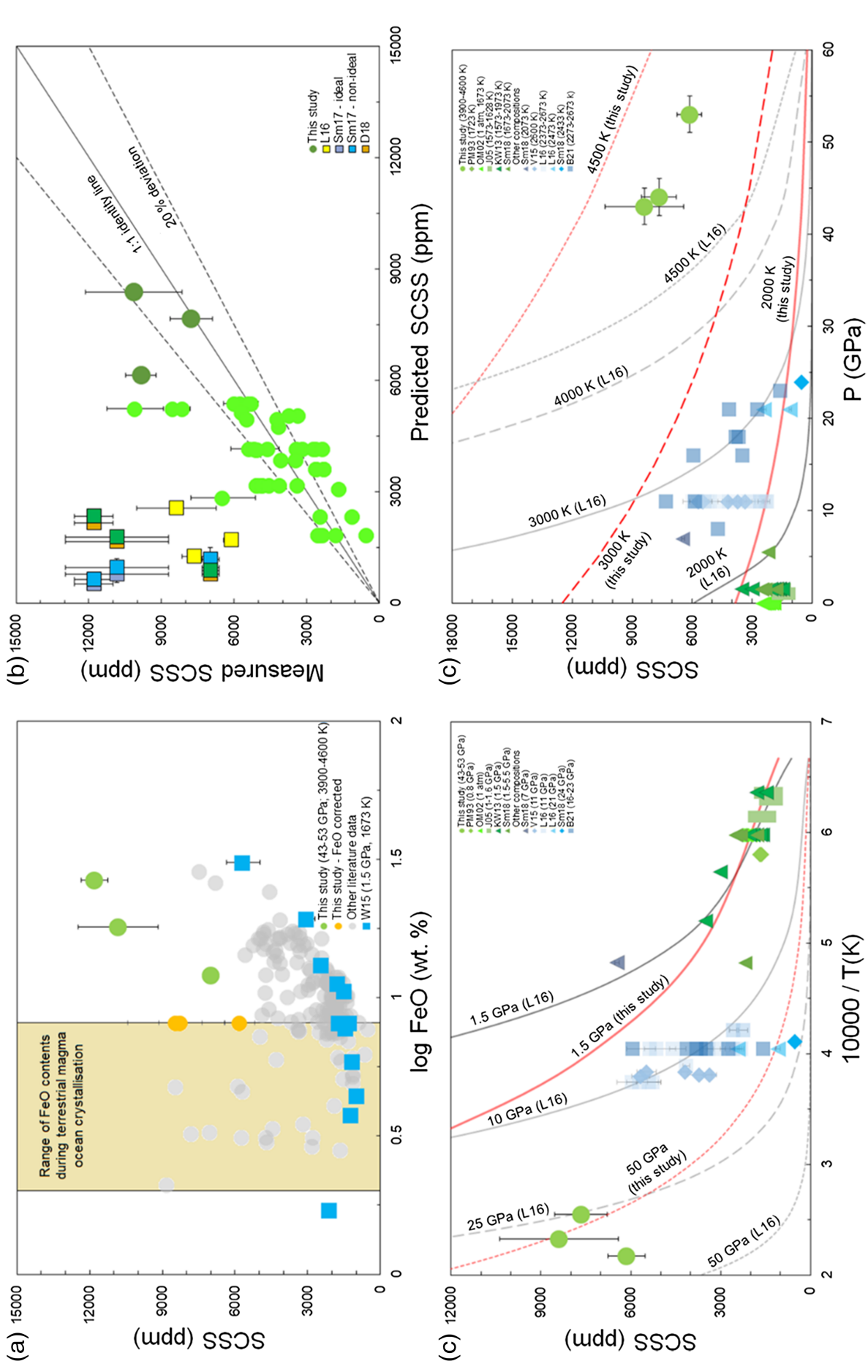

Figure 2 Newly derived SCSS values and FeO-normalised SCSS values (normalised to 8.1 wt. % FeO or $X_{FeO}^{sil\,melt} = 0.05$, using the model of Steenstra *et al.* (2018) (Supplementary Information). **(a)** SCSS *versus* FeO content of the silicate melt. **(b)** Comparison between measured and predicted SCSS values calculated using previous models. The SCSS values of the peridotitic L16 model are compared with our SCSS data normalised to the same FeO content as used for that model (8.1 wt. % FeO). The measured and compared values of other SCSS models were based on measured FeO contents. Light green symbols indicate other FeO-normalised literature data which were compared with the model of Equation 2 (Table S-2). **(c–d)** The FeO-normalised SCSS as a function of *P-T*. Grey and red lines indicate the *P-T* dependencies of the L16 peridotite SCSS model and our new model (Eq. 2), respectively. Literature data and/or previous models from Kiseeva and Wood (2013, 2015); Vogel *et al.* (2015); Laurenz *et al.* (2016); Smythe *et al.* (2017); Ding *et al.* (2018); Blanchard *et al.* (2021) (Table S-2).

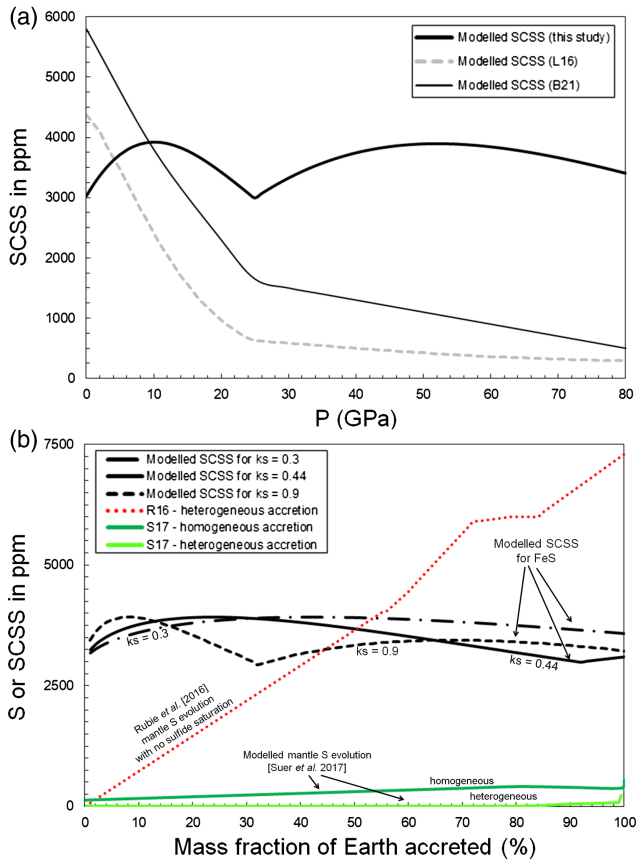

Figure 3 **(a)** Variation of the SCSS during terrestrial magma ocean crystallisation along a geotherm ranging approximately midway between the peridotite solidus and liquidus (Rubie *et al.*, 2015; Eqs. S-2,3). Plotted for comparison are previous peridotite SCSS models (Laurenz *et al.*, 2016; Blanchard *et al.*, 2021). **(b)** Calculated SCSS values for various average effective pressures of sulfide saturation (kS; Rubie *et al.*, 2016; Eq. S-4) as a function of accreted mass.

reported (*e.g.*, Blanchard *et al.*, 2021), whereas the derived negative temperature term is considerably lower than the high-pressure models (Laurenz *et al.*, 2016; Smythe *et al.*, 2017). It is, however, larger than currently available low-pressure models (Ding *et al.*, 2018; Steenstra *et al.*, 2018) as well as the high-pressure model of Blanchard *et al.* (2021). Our modelling results thus suggest significantly higher SCSS values for the terrestrial magma ocean at high *P-T* conditions (Fig. 3a).

Implications for the Terrestrial Sulfur Cycle

In Figure 3b, the new SCSS model is incorporated in Earth accretion models from previous studies (Rubie *et al.*, 2016; Tagawa *et al.*, 2021), while exploring different average effective pressures of sulfide saturation or kS (Eq. S-4). The range of kS considered here is based on the preferred value of Rubie *et al.* (2016) (kS = 0.44) while exploring the sensitivity of the results to different kS values. Figure 3b shows that for the mantle S contents modelled by Rubie *et al.* (2016) sulfide saturation in the magma ocean will most certainly occur at approximately 55 % of magma ocean crystallisation. This conclusion is virtually independent of the assumed effective pressure of FeS saturation and would imply a major S reservoir in the deep mantle in addition to the core itself. This is also consistent with mantle HSE systematics (Laurenz *et al.*, 2016; Rubie *et al.*, 2016). In contrast, the modelled mantle S evolution curves from Suer *et al.* (2017) are much lower relative to modelled SCSS values. Here, the mantle S content is insufficient to yield sulfide saturation at any stage of magma ocean crystallisation, especially if one considers the slightly higher SCSS values expected for a peridotite liquid (Fig. 3b). The large differences between the mantle S evolution models of Rubie *et al.* (2016) and Suer *et al.* (2017) are due to the fact that they considered very different accretion models. The first model considers accretion of a fraction of undifferentiated planetesimals (*i.e.* fully oxidised) with low degrees of terrestrial core-mantle re-equilibration, whereas in the second model all accreted bodies are differentiated and equilibrated at low *P-T* conditions and their cores experienced further partial re-equilibration in the deep terrestrial magma ocean. If modelled S abundances for the terrestrial magma ocean of Suer *et al.* (2017) are correct, our results imply that sulfide saturation could not have occurred during magma ocean crystallisation, or perhaps only very late (>99.9 %) when the very last residual liquid is extremely enriched in S. The absence of, or very late, sulfide saturation of the residual magma ocean is problematic in terms of transporting sulfide liquid to the deep mantle as proposed to explain HSE systematics (Rubie *et al.*, 2016), given the limited percolation of FeS liquid through a crystalline upper mantle (Terasaki *et al.*, 2008). Although interconnection of FeS liquid occurs at lower mantle conditions (Shi *et al.*, 2013), it is unlikely that such late segregated FeS liquid would be transportable to the lower mantle and that global HSE depletions would be established at such late stages of magma ocean crystallisation (Fig. 3b). The S evolution models of Suer *et al.* (2017) do reproduce the current S content of the bulk silicate Earth, and given the highly chalcophile affinities of the HSE (Laurenz *et al.*, 2016), only very minor amounts of sulfides would be required to establish primitive mantle HSE depletions. Overall, our results show that either the magma ocean must have been very rich in S to achieve sulfide saturation as proposed to satisfy HSE abundance constraints (Rubie *et al.*, 2016) or that, instead, iron disproportionation affected HSE systematics in the early Earth (Suer *et al.*, 2021).

Acknowledgements

This work was supported by a Carnegie Postdoctoral Fellowship awarded to E.S.S. OTL acknowledges support from the Royal Society in the form of a University Research Fellowship (UF150057). We thank two anonymous reviewers for their useful comments which greatly improved the quality of the manuscript and would like to thank Maud Boyet for editorial handling.

Editor: Maud Boyet

Additional Information

Supplementary Information accompanies this letter at https://www.geochemicalperspectivesletters.org/article2219.

Cite this letter as: Steenstra, E.S., Lord, O.T., Vitale, S., Bullock, E.S., Klemme, S., Walter, M. (2022) Sulfur solubility in a deep magma ocean and implications for the deep sulfur cycle. *Geochem. Persp. Let.* 22, 5–9. https://doi.org/10.7185/geochemlet.2219

References

Blanchard, I., Siebert, J., Borensztajn S., Badro, J. (2017) The solubility of heat-producing elements in Earth's core. *Geochemical Perspective Letters* 5, 1–5. https://doi.org/10.7185/geochemlet.1737

Blanchard, I., Abeykoon, S., Frost, D.J., Rubie, D.C. (2021) Sulfur content at sulfide saturation of peridotitic melt at upper mantle conditions. *American Mineralogist* 106, 1835–1843. https://doi.org/10.2138/am-2021-7649

Boujibar, A., Andrault, D., Bouhifd, M.A., Bolfan-Casanova, N., Devidal, J.-L., Trcera, N. (2014) Metal-silicate partitioning of sulphur, new experimental and thermodynamic constraints on planetary accretion. *Earth and Planetary Science Letters* 391, 42–54. https://doi.org/10.1016/j.epsl.2014.01.021

Boukare, C.-E., Parman, S.W., Parmentier, E.M., Anzures, B.A. (2019) Production and Preservation of Sulfide Layering in Mercury's Mantle. *Journal of Geophysical Research: Planets* 124, 3354–3372. https://doi.org/10.1029/2019JE005942

Callegaro, S., Geraki, K., Marzoli, A., de Min, A., Maneta, V., Baker, D.R. (2020) The quintet completed: the partitioning of sulfur between nominally volatile-free minerals and silicate melts. *American Mineralogist* 105(5), 697–707. https://doi.org/10.2138/am-2020-7188

Ding, S., Hough, T., Dasgupta R. (2018) New high-pressure experiments on sulfide saturation of high-FeO* basalts with variable TiO_2 contents - Implications for the sulfur inventory of the lunar interior. *Geochimica Cosmochimica Acta* 222, 319–339. https://doi.org/10.1016/j.gca.2017.10.025

Huang, D., Badro, J., Siebert, J. (2020) The niobium and tantalum concentration in the mantle constraints the composition of Earth´s primordial magma ocean. *Proceedings of the National Academy of Sciences* 117, 27893–27898. https://doi.org/10.1073/pnas.2007982117

Laurenz, V., Rubie, D.C., Frost, D.J., Vogel, A.K. (2016) The importance of sulfur for the behavior of highly-siderophile elements during Earth's differentiation. *Geochimica et Cosmochimica Acta* 194, 123–138. https://doi.org/10.1016/j.gca.2016.08.012

Kiseeva, E.S., Wood, B.J. (2013) A simple model for chalcophile element partitioning between sulphide and silicate liquids with geochemical applications. *Earth and Planetary Science Letters* 383, 68–81. https://doi.org/10.1016/j.epsl.2013.09.034

Kiseeva, E.S., Wood, B.J. (2015) The effects of composition and temperature on chalcophile and lithophile element partitioning into magmatic sulphides. *Earth and Planetary Science Letters* 424, 280–294. https://doi.org/10.1016/j.epsl.2015.05.012

Namur, O., Charlier, B., Holtz, F., Cartier, C., McCammon, C. (2016) Sulfur solubility in reduced mafic silicate melts: Implications for the speciation and distribution of sulfur on Mercury. *Earth and Planetary Science Letters* 448, 102–114. https://doi.org/10.1016/j.epsl.2016.05.024

O'Neill, H.St.C. (1991) The origin of the Moon and the early history of the Earth – A chemical model. Part 2: the Earth. *Geochimica et Cosmochimica Acta* 55, 1159–1172. https://doi.org/10.1016/0016-7037(91)90169-6

O'Neill, H.St.C., Mavrogenes, J.A. (2002) The sulfide capacity and the sulfur content at sulfide saturation of silicate melts at 1400°C and 1 bar. *Journal of Petrology* 43, 1049–1087. https://doi.org/10.1093/petrology/43.6.1049

Palme, H., O'Neill, H.St.C (2014) 3.1 - Cosmochemical estimates of mantle composition. In: Holland, H.D., Turekian, K.K. (Eds.) *Planets, Asteroids, Comets and The Solar System, Treatise of Geochemistry (Second Edition)*. Elsevier, Oxford, 1–39. https://doi.org/10.1016/B978-0-08-095975-7.00201-1

Rubie, D.C., Jacobson, S.A., Morbidelli, A., O'Brien, D.P., Young, E.D., de Vries, J., Nimmo, F., Palme, H., Frost, D.J. (2015) Accretion and differentiation of the terrestrial planets with implications for the compositions of early-formed Solar System bodies and accretion of water. *Icarus* 248, 89–108. https://doi.org/10.1016/j.icarus.2014.10.015

Rubie, D.C., Laurenz, V., Jacobson, S.A., Morbidelli, A., Palme, H., Vogel, A.K., Frost, D.J. (2016) Highly siderophile elements were stripped from Earth's mantle by iron sulfide segregation. *Science* 353, 1141–1144. https://doi.org/10.1126/science.aaf6919

Shi, C.Y., Zhang, L., Yang, W., Liu, Y., Wang, J., Meng, Y., Andrews, J., Mao, W. (2013) Formation of an interconnected network of iron melt at Earth´s lower mantle conditions. *Nature Geoscience* 6, 971–975. https://doi.org/10.1038/ngeo1956

Smythe, D.J., Wood, B.J., Kiseeva, E.S. (2017) The S content of silicate melts at sulfide saturation: New experiments and a model incorporating the effects of sulfide composition. *American Mineralogist* 102, 795–803. https://doi.org/10.2138/am-2017-5800CCBY

Steenstra, E.S., Seegers, A.X., Eising, J., Tomassen, B.G.J., Webers, F.P.F., Berndt, J., Klemme, S., Matveev, S., van Westrenen, W. (2018) Evidence for a sulfur undersaturated lunar interior from the solubility of sulfur in lunar melts and sulfide-silicate partitioning of siderophile elements. *Geochimica et Cosmochimica Acta* 231, 130–156. https://doi.org/10.1016/j.gca.2018.04.008

Steenstra, E.S., Berndt, J., Klemme. S., Snape, J.F., Bullock. E.S., van Westrenen, W. (2020a) The fate of sulfur and chalcophile elements during crystallization of the lunar magma ocean. *Journal of Geophysical Research: Planets* 125, e2019JE006328. https://doi.org/10.1029/2019JE006328

Steenstra, E.S., Berndt, J., Klemme, S., Rohrbach, A., Bullock, E.S., van Westrenen, W. (2020b) An experimental assessment of the potential of sulfide saturation of the source regions of eucrites and angrites: implications for asteroidal models of core formation, late accretion and volatile element depletions. *Geochimica et Cosmochimica Acta* 269, 39–62. https://doi.org/10.1016/j.gca.2019.10.006

Suer, T.-A., Siebert, J., Remusat, L., Menguy, N., Fiquet, G. (2017) A sulfur-poor terrestrial core inferred from metal-silicate partitioning experiments. *Earth and Planetary Science Letters* 469, 84–97. https://doi.org/10.1016/j.epsl.2017.04.016

Suer, T.-A., Siebert, J., Remusat, L., Day, J.M.D., Borensztajn, S., Doisneau, B., Fiquet, G. (2021) Reconciling metal-silicate partitioning and late accretion in the Earth. *Nature Communications* 12, 2913. https://doi.org/10.1038/s41467-021-23137-5

Tagawa, S., Sakamoto, N., Hirose, K., Yokoo, S., Hernlund, J., Ohishi, Y., Yurimoto, H. (2021) Experimental evidence for hydrogen incorporation into Earth's core. *Nature Communications* 12, 2588. https://doi.org/10.1038/s41467-021-22035-0

Terasaki, H., Frost, D.J., Rubie, D.C., Langenhorst, F (2008) Percolative core formation in planetesimals. *Earth and Planetary Science Letters* 273, 132–137. https://doi.org/10.1016/j.epsl.2008.06.019

Vogel, A.K. (2015) Siderophile element partitioning at high pressures and temperatures: implications for core formation processes. PhD thesis, Universität Bayreuth, Germany. http://nbn-resolving.org/urn:nbn:de:bvb:703-epub-2039-3

Walter, M.J., Thomson, A.R., Wang, W., Lord, O.T., Ross, J., McMahon, S.C., Baron, M.A., Melekhova, E., Kleppe, A.K., Kohn, S.C. (2015) The stability of hydrous silicates in Earth's lower mantle: Experimental constraints from the systems $MgO\text{-}SiO_2\text{-}H_2O$ and $MgO\text{-}Al_2O_3\text{-}SiO_2\text{-}H_2O$. *Chemical Geology* 418, 16–29. https://doi.org/10.1016/j.chemgeo.2015.05.001

Wykes, J.L., O'Neill, H.St.C, Mavrogenes, J.A. (2015) The effect of FeO on the sulfur content at sulfide saturation (SCSS) and the selenium content at selenide saturation of silicate melts. *Journal of Petrology* 56, 1407–1424. https://doi.org/10.1093/petrology/egv041

Geochemical Perspectives Letters

Sulfur solubility in a deep magma ocean and implications for the deep sulfur cycle

E.S. Steenstra, O. Lord, S. Vitale, E.S. Bullock, S. Klemme, M. Walter

Supplementary Information

The Supplementary Information includes:

- S.1 Experimental and Analytical Details
- S.2 Evidence for Sulfide-saturation of Experimental Silicate Melts
- S.3 Correcting SCSS values for Variable Silicate Melt FeO Contents
- S.4 Non FeO-compositional Effects on Derived SCSS values
- S.5 Dataset used for Parameterisations
- S.6 Modelling Approach
- Tables S-1 and S-2
- Figures S-1 to S-3
- Supplementary Information References

S.1 Experimental and Analytical Details

To study the solubility of S in a deep terrestrial magma ocean, sulfide liquids and silicate melts were equilibrated at pressures of 35–40 GPa and temperatures between 3925–4600 K in a laser-heated diamond anvil cell (DAC). The sulfide powder consisted of FeS and 3 wt. % of trace elements (ESS-DAC-4: FeS + 2 wt. % Cu and 1 wt. % Se; ESS-DAC-5: FeS + 2 wt. % Cu and 1 wt. % Te; ESS-DAC-7: FeS + 1.5 wt. % Cd and 1.5 wt. % Sn). The silicate powder consisted of a grounded (from glass), synthetic equivalent of a mean MORB basaltic composition (Table S-1, Gale *et al.*, 2013). The MORB silicate composition was used because it quenches to a glass and because its melting temperature is significantly lower than more magnesian compositions. In addition, it also allows for direct comparison with data that was obtained over

much larger *P-T* ranges due to its lower melting point and extensive use in past low-pressure studies. The glass was produced by mixing the appropriate amounts of high-purity carbonates and oxides under ethanol in an agate mortar for 30 minutes. The mixture was then decarbonated over 6-7 hours from 923 to 1273 K, taken from the furnace and subsequently melted at 1723 K for 15 minutes in a box furnace.

Experiments were performed in Princeton-type symmetric cells, equipped with anvils with culets of 250 µm diameter. Sample chambers of diameter 85 µm were laser drilled in 250 µm thick Re gaskets pre-indented to a thickness of 50 µm. Powdered starting materials were pressed between two opposing diamonds with culet diameters of 500 µm to produce thin foils ~10 to 15 µm thick. A piece of the sulfide wafer ~20 µm across was loaded into the sample chamber between pieces of the MORB wafer chosen to closely match the diameter of the sample chamber. In this geometry, the MORB acts as the pressure medium and thermal insulation.

The fluorescence signal from a ruby grain loaded into the sample chamber but away from the heated region was used to monitor the pressure during pressurisation and after heating. Pressures were calculated using two different approaches. In the first method the reported pressures are the average between pre-heating and post-heating measurements. In the second approach, we took into account the potentially important thermal pressure effects using the parameterisation of Siebert *et al.* (2012):

$$\Delta Pth \sim 2.7^{-3}\ GPa/K \qquad Eq.\ (S\text{-}1)$$

These calculations showed pressures were between 43 to 53 GPa during the experiment (Table 1 in the main text); these values were used throughout the study. The pressure uncertainty is estimated to be approximately 2 GPa at the conditions of the experiments (Walter *et al.*, 2015). Samples were heated at high pressure using the double-sided pulsed laser heating system at the School of Earth Sciences, University of Bristol and described in detail in Lord *et al.* (2014). Samples were heated with a pair of 100-W Yb-doped fibre lasers for approximately 60 to 180 seconds, by switching on the lasers at a high power during which a steady state must have been achieved, given previous results for LH-DAC partitioning experiments (*e.g.* Suer *et al.*, 2017; Mahan *et al.*, 2018). Samples were quenched by switching off the power to the lasers. During this period, multiple 1-D temperature transects were measured across both sides of the heated spot using the optical system also described in Lord *et al.* (2014) and standard spectroradiometric techniques (Walter and Koga, 2004). Reported temperatures are an average of the peak temperatures of each of these transects and the reported uncertainty is their standard deviation.

Recovered experimental run products were mounted on Si wafers. Cross-sections of experimental charges were made using a dual beam FEI Helios G4 Xe PFIB at the Earth and Planets Laboratory, Carnegie Institution for Science. A 5 µm protective layer of tungsten (W) was deposited on to the sample surface. Standard FIB cross sectioning techniques were used over a current range of 60 nA to 2.5 µA. Samples were finished with 30 kV Xe ions. Final sample thicknesses were approximately 20 µm. Run products were carbon-coated and analysed using an EPMA at the latter institution.

Major and trace element compositions of the silicate melts and/or sulfide liquids were obtained using a JEOL JXA 8530F field emission electron microprobe at the Earth and Planets Laboratory, Carnegie Institution for Science. Analyses were performed using a defocused beam of mostly 1 µm and occasionally 3 µm diameter. Measurement points were set in random lines and/or raster grids, depending on the available surface area of the analysed phases. Beam currents were 20 nA with an accelerating voltage of 15 kV. Dwell times were 10–40 s on peak and 5–20 s on each background. Standards used were anorthite for Ca, Fe metal or fayalite for Fe, San Carlos olivine for Si, orthoclase for K, albite or DJ35 for Na, PbS or pyrite for S, TiO_2 or pure metal for TiO_2, SnSe for Se, CdTe for Cd and pure metal standards for Cu, and Re. Calibrations were considered successful when the primary standard compositions were reproduced within 1% relative

deviation. Data reduction was performed using the ZAF correction, which corrects for the decrease in x-ray density due to the distance the x-rays travel through the specimen before they reach the detector. In runs ESS-4 and ESS-5 the sulfide liquid was either too small to measure or migrated too far from the hotspot due to its very low viscosity at such conditions.

Special care was taken to not measure too close to sulfide liquid (>15 µm, and usually much further away), as this would potentially yield secondary fluorescence effects on measured S abundances, as observed for other elements such as Ni (Wade and Wood, 2012). Wafer (sample) thickness may also result in analytical uncertainties, as not all photons that are emitted would arrive at the detector, due to deeper penetration of electrons beyond the wafer thickness. Wade and Wood (2012) showed that this would be most significant for the heaviest elements of interest; in our case Ca, Ti and Fe. First, it is observed that TiO_2 contents are actually increased relative to the starting materials (Table S-1), suggesting no significant ‘’unmeasured’’ TiO_2. Although CaO contents are decreased relative to the starting composition, this is due to the crystallisation of Ca-perovskite close to the melt - solid interface, forming a characteristic CaO-, SiO_2-enriched and FeO-, Al_2O_3-depleted rim (Fig. S-1 to S-3; see also Tagawa *et al.*, 2021). We therefore concluded that none of the EPMA measurements were affected by wafer thickness issues. The low total of ESS-DAC-7 is therefore also not related to wafer thickness issues, but perhaps by some Na_2O loss under the beam. It should be noted that the majority of literature SCSS experiments have low totals – the compiled dataset of Steenstra *et al*. (2018) yields an average of 98.70 ± 1.61 (1SD) obtained for a wide variety of capsule types and set-ups – which is probably a result of the increased analytical challenges of measuring S-rich silicate melts (see Steenstra *et al.*, 2020a for a detailed discussion on this topic).

S.2 Evidence for Sulfide-saturation of Experimental Silicate Melts

For the application of our results, it is important to demonstrate that the silicate melts are indeed sulfide-saturated and that they do not simply represent a melt that fully consumed the available sulfide liquid at the heated spot. Several lines of evidence can be used to argue for sulfide saturation. The most important line of evidence that argues for sulfide saturation of the experimental silicate melts at high *P-T* is the sign and magnitude of the variation of the SCSS with the FeO content of the silicate melt (Fig. 2a). Although there are slight *P-T* differences between the experiments, the SCSS versus wt. % FeO slope is very similar to/within error of systematic low pressure experimental observations by Wykes *et al*. (2015). The slope is also consistent with theoretical thermodynamic considerations of the increased dominance of the sulfide capacity term over other terms at higher FeO contents (>4 wt. % FeO; Wykes *et al.*, 2015). Given the fact that post-run FeS generally migrated to the edges of the heated spot, suggests the silicate melt either equilibrated with sulfide through liquid channels or that when it segregates it leaves a sulfide-saturated melt. The latter would be consistent with the expected, extremely fast diffusion of S in silicate melts at the very high temperatures of the experiments (Zhang *et al.*, 2010). In the unlikely case that the experimental silicate melts were not sulfide-saturated at high *P-T* conditions, our results provide important lower limits which are already are dramatically higher than modeled values using previous SCSS models. Finally, sulfide liquids generally migrated from the heated spot to colder areas, so that it cannot be excluded that FeS liquids initially present at peak conditions have slightly lower S contents relative to stoichiometric FeS (xFeS < 1). As SCSS increases with xFeS (*e.g.* Smythe *et al.*, 2017), any deviation from xFeS = 1 would only further increase the relative differences between low- and high pressure results.

S.3 Correcting SCSS Values for Variable Silicate Melt FeO Contents

To unravel the effects of *P-T* on the SCSS, the data from this study and previous literature data from otherwise highly similar compositions should be normalised to a common FeO content, as FeO is by far the most important silicate melt compositional variable affecting the SCSS (*e.g.* O’Neil and Mavrogenes, 2002). We therefore used the FeO term from Table 5 of Steenstra *et al.* (2018) (CX_{Fe} = 2.15(40)), which was

derived from consideration of an extensive SCSS dataset (N = 337) and also incorporated sulfide compositional effects. Both the literature data and our newly derived high P-T data was normalised to $x_{\mathrm{FeO}}^{sil\,melt}$ = 0.05, corresponding to 8.1 wt. % FeO i.e. the FeO content of the present-day terrestrial primitive mantle (Palme and O´Neill, 2014). To incorporate any uncertainties arising from this correction, we propagated the uncertainties on both the FeO parameter form Steenstra *et al.* (2018) and on the actual measured SCSS values. This increased the uncertainties of the new high P-T SCSS values by 150 to 300 ppm, depending on the experiment. It should be noted that the SCSS does not vary significantly (200–300 ppm) between approximately 2 to 8 wt. % FeO, virtually the full range of potential FeO contents during terrestrial magma ocean crystallisation, as this is the minimum of the parabolic behavior describing SCSS as a function of FeO content (Wykes *et al*., 2015; Fig. 2a in the main text).

S.4 Non FeO-compositional Effects on Derived SCSS Values

A MORB composition was chosen for the experiments because of its relatively low melting temperature and propensity for quenching to a glass (*e.g.* Suer *et al.,* 2017; Mahan *et al.,* 2018). The MORB composition (Gale *et al.,* 2013) used in our study is, however, significantly different than the expected composition of a primitive terrestrial magma ocean liquid or the primitive mantle (*e.g.* Palme and O'Neill, 2014). It should be noted that differences in FeO contents between our experiments and previous studies were taken into account by applying the FeO correction term from Steenstra *et al.* (2018), which is CX_{Fe} = 2.15(40) (see section S.3). Note that the magnitude of the FeO effect is very similar for all previous SCSS models (*e.g.* Smythe *et al.,* 2017; Ding *et al.,* 2018, Steenstra *et al.,* 2018). Using the Smythe *et al.* (2017) model, we calculate the potential difference for an 8.1 wt. % FeO bearing primitive mantle melt (assuming the primitive mantle or PM composition from Palme and O'Neill, 2014) and compare the calculated SCSS value with SCSS values calculated for our experimental liquid compositions, normalised to 8.1 wt. % FeO. These calculations at 1 GPa and 1873 K suggests that the PM SCSS value is 850–1220 ppm higher than for the experimental liquid compositions. The SCSS for a peridotite-type liquid would thus only be slightly higher at the experimental P-T conditions, and confirms FeO is the main silicate melt compositional parameter affecting the SCSS, consistent with previous observations (*e.g.* Wykes *et al.,* 2015, Steenstra *et al.*, 2020a).

S.5 Dataset used for Parameterisations

To remove any potential effects arising from different silicate melt compositions, we use the following criteria and exclude the following literature data from our statistical database (1) H_2O-rich SCSS experiments, as each wt. % H_2O will result in an approximate increase of the SCSS by 100 ppm (Fortin *et al.,* 2015); (2) all SCSS data for silicate melts with <2.5 wt. % FeO due to the anomalous slope of SCSS versus FeO at low FeO contents (*e.g.* Wykes *et al.,* 2015; Steenstra *et al.,* 2020b); (3) all SCSS data for silicate melts with >2.5 wt. % TiO_2 due to the effects of high-Ti contents on the slope of SCSS with FeO (O'Neill and Mavrogenes, 2002); (4) all SCSS data for silicate melts with >55 wt. % SiO2 due to the effects of SiO_2 on the SCSS (*e.g.* O'Neill and Mavrogenes, 2002; Smythe *et al.,* 2017; Steenstra *et al.,* 2018); (5) all SCSS data with >2.6 wt. % of alkalis due to their negative effects on the SCSS (D'Souza and Canil, 2018); (6) all SCSS data for silicate melts that have more than ±5 wt. % CaO, Al_2O_3 and ±2.5 wt. % MgO difference between the average compositions of our experiments; (7) all SCSS data for Fe-S liquid with <30 wt. % S due to the negative effects of lower sulfide xFeS on the SCSS (Smythe *et al.,* 2017) and (8) all SCSS data for Fe-S liquid with > ±6 wt. % of trace elements due to the negative effects of lower xFeS on the SCSS, which may vary with the type of element considered. In the end, 42 SCSS values were included in the regression, with an overall P-T range of 1 atm to 40 GPa and T = 1573–4605 K, which are listed in Supplementary Table S-1.

S.6 Modelling Approach

To model the SCSS in a deep terrestrial magma ocean, we used main-text Eq. 2 in conjunction with the multi-stage core formation model (#S1) reported by Tagawa *et al.* (2021), which was directly based on the Rubie *et al.* (2015) model. Equation 2 is based on a primitive mantle content of 8.1 wt. % FeO and does not include an FeO term, as the SCSS does not deviate significantly within the FeO range relevant for the terrestrial magma ocean (*e.g.* Rubie *et al.*, 2015). It should be noted that in the latter models the FeO content is slightly lower in the first few % of magma ocean crystallisation if highly reduced accretion is assumed to have occurred early. This could hypothetically yield somewhat different SCSS values within the first few % of terrestrial accretion, but at this stage S contents are low and the SCSS would only be increased relative to higher FeO contents, making sulfide saturation also highly unlikely at this stage. The assumed geotherms, taken from Rubie *et al.* (2015) and required for calculating the SCSS values in Fig. 3a-b are based on liquidus/solidus data and were specifically calibrated for modeling the geotherms for magma ocean pressures below and above 24 GPa, respectively:

$$P < 24\ \text{GPa}: T_e = 1874 + 55.43P - 1.74P^2 + 0.0193P^3 \qquad \text{Eq. (S-2)}$$

$$P \geq 24\ \text{GPa}: T_e = 1249 + 58.28P - 0.395P^2 + 0.0011P^3 \qquad \text{Eq. (S-3)}$$

The modelled limit of 80 GPa corresponds with the proposed maximal pressure for a basal magma ocean (De Vries *et al.*, 2016). We incorporated the S mantle evolution model depicted in Fig. 1 from Rubie *et al.* (2015), as well as the models from Suer *et al.* (2017), which are based on either homogeneous or heterogeneous accretion. We compare these estimates with the modeled SCSS values (Eq. 2) while assuming different effective pressures of sulfide saturation, as a function of accreted mass %. The pressure versus accreted mass relationship was taken from Tagawa *et al.* (2021).

Rubie *et al.* (2015) defined the following equation for the average effective pressure of sulfide saturation, as sulfide segregation may occur at different depths in the magma ocean at a given stage of accretion:

$$\text{Peq-S} = \text{kS} \times \text{PCMB} \qquad \text{Eq. (S-4)}$$

where PCMB is the core-mantle boundary pressure at the time of each FeS exsolution event, and kS is a constant (Rubie *et al.*, 2015).

Supplementary Tables

Table S-1 Composition of the silicate starting glass and experimentally produced melts as measured by electron microprobe. *N* represents the number of analyses.

	SiO_2 (wt. %)	MgO	Al_2O_3	CaO	FeO	TiO_2	Na_2O	K_2O	CuO	CdO	ReO_2	S	Sum	*N*
Silicate melts														
Starting composition	48.48(14)	7.88(4)	15.17(3)	11.43(4)	9.79(5)	1.70(1)	2.54(2)	0.156(4)	–	–	–	–	97.36(15)	15
ESS-DAC-4	43.43(72)	8.63(18)	18.42(33)	7.94(6)	12.59(26)	1.89(2)	1.52(47)	0.135(5)	0.95(3)	–	0.05(3)	0.70(4)	96.25(96)	5
ESS-DAC-5	36.02(50)	8.48(11)	22.63(31)	6.51(8)	18.05(59)	1.44(2)	1.58(3)	0.066(4)	1.18(3)	–	0.10(6)	1.08(21)	97.14(63)	19
ESS-DAC-7	34.00(28)	7.69(7)	13.15(17)	6.85(6)	26.54(43)	2.32(1)	1.92(2)	0.144(3)	0.02(1)	0.286(4)	0.03(1)	1.18(8)	94.12(16)	32
	Fe (wt. %)	**S**	**Na**	**Mg**	**Si**	**Al**	**Ca**	**Ti**	**Cu**	**Re**	**Se**	**O**	**Sum**	***N***
Sulfide liquid														
ESS-DAC-4	55.89(381)	26.32(176)	0.26(18)	0.31(13)	1.09(146)	1.20(55)	0.52(72)	0.09(4)	1.35(158)	0.21(22)	n.d.	6.23(188)	93.68(214)	3

Table S-2 Compilation of used literature data.

Table S-2 is available for download (Excel) at https://doi.org/10.7185/geochemlet.2219

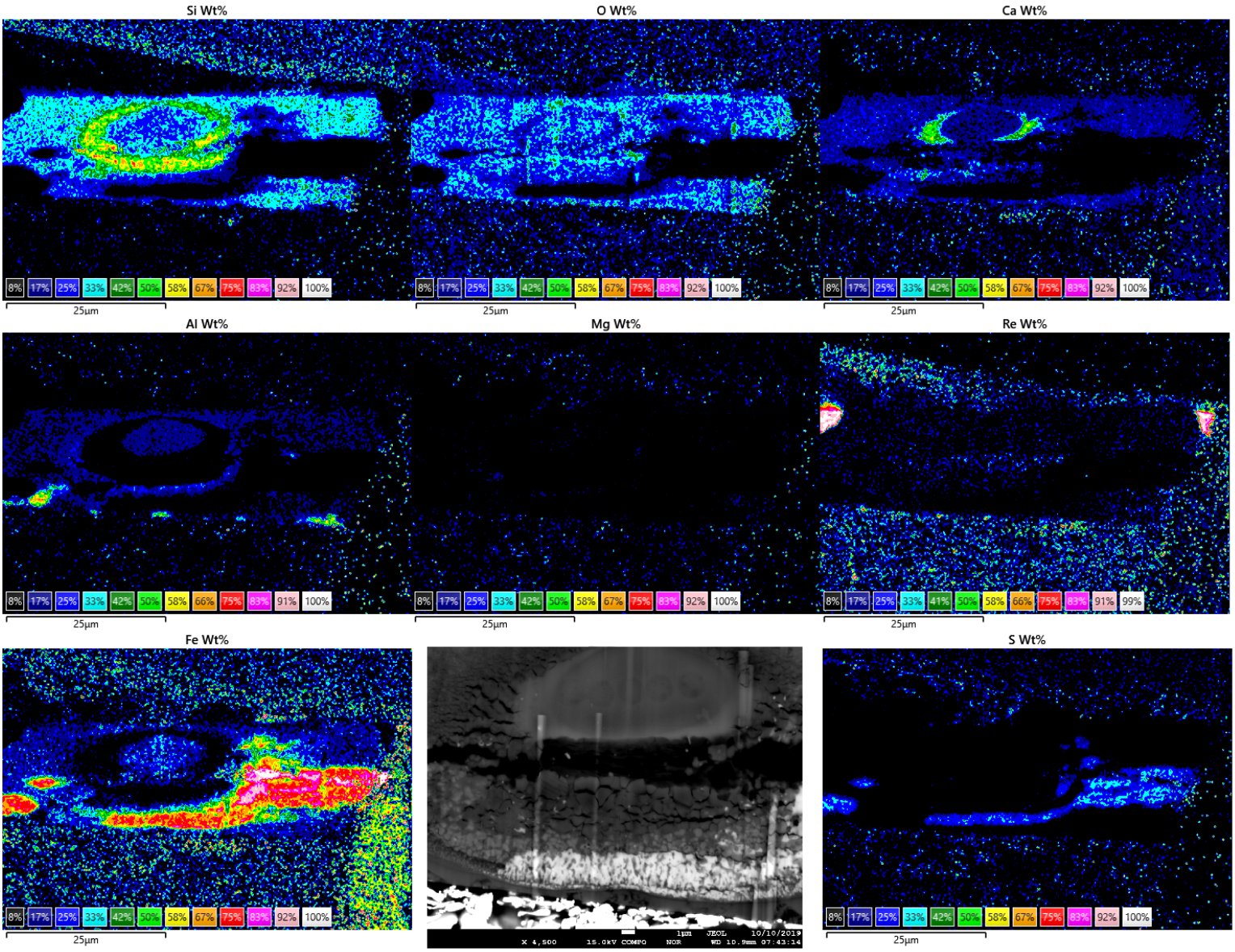

Figure S-1 Elemental EDS maps of experiment ESS-4-DAC.

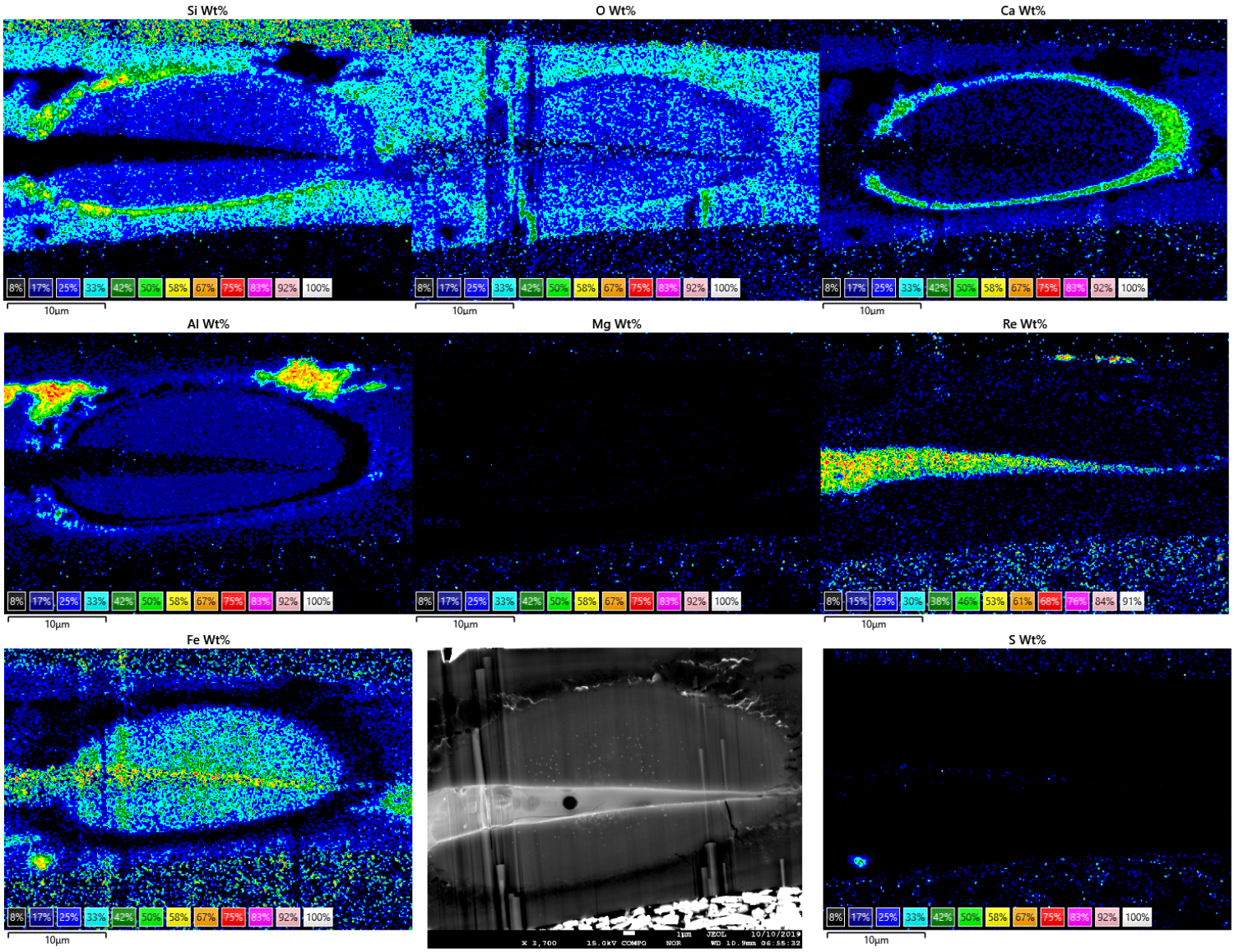

Figure S-2 Elemental EDS maps of experiment ESS-5-DAC.

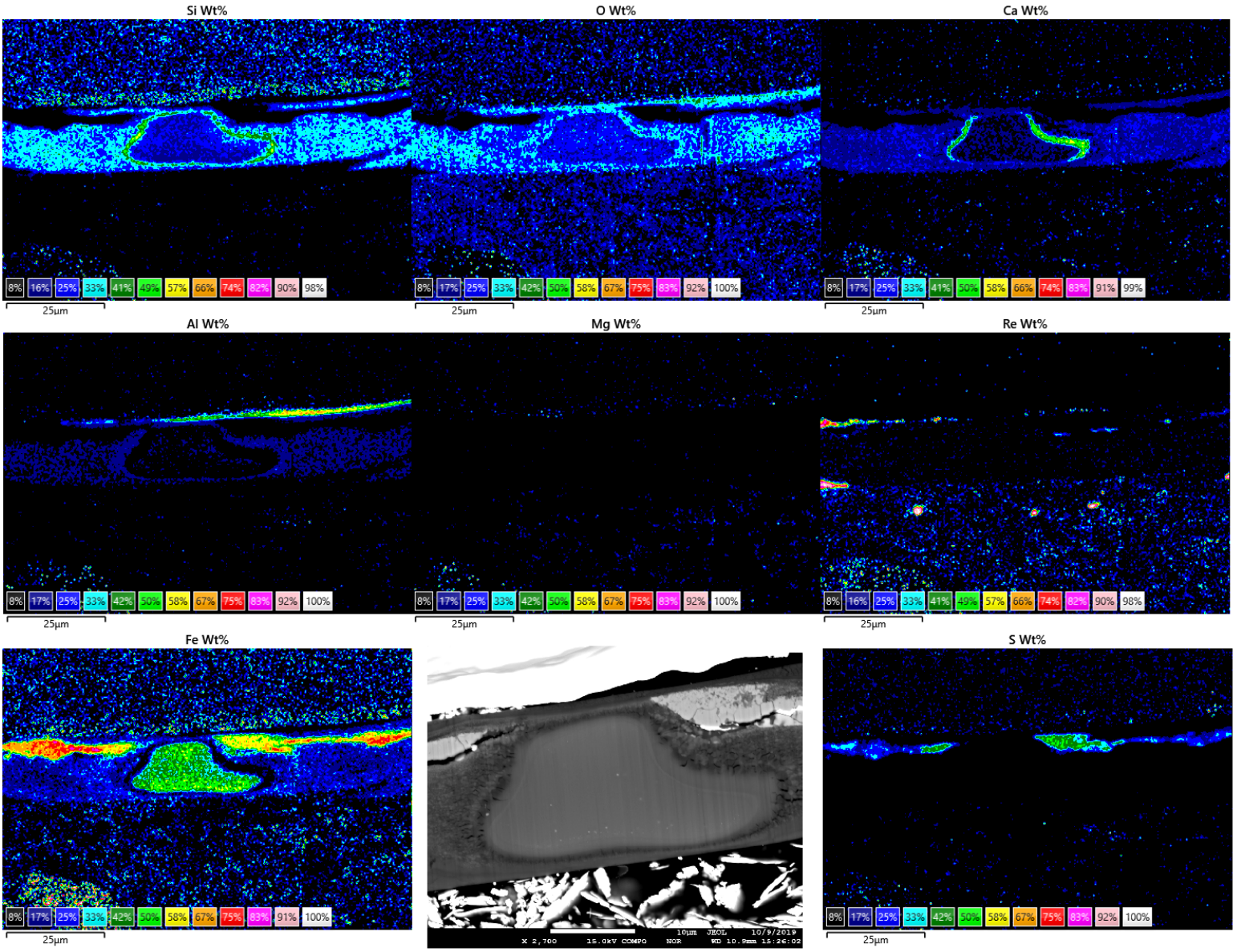

Figure S-3 Elemental EDS maps of experiment ESS-7-DAC.

Supplementary Information References

De Vries, J., Nimmo, F., Melosh, H.J., Jacobson, S.A., Morbidelli, A., Rubie, D.C. (2016) Impact-induced melting during accretion of the Earth. *Progress in Earth and Planetary Science* 3, 7. https://doi.org/10.1186/s40645-016-0083-8

Ding, S., Hough, T., Dasgupta, R. (2018) New high-pressure experiments on sulfide saturation of high-FeO* basalts with variable TiO_2 contents - Implications for the sulfur inventory of the lunar interior. *Geochimica et Cosmochimica Acta* 222, 319–339. https://doi.org/10.1016/j.gca.2017.10.025

D'Souza, R.J., Canil, D. (2018) Effect of alkalinity on sulfur concentration at sulfide saturation in hydrous basaltic andesite to shoshonite melts at 1270°C and 1 GPa. *American Mineralogist* 103, 1030–1043. https://doi.org/10.2138/am-2018-6404

Fortin, M.-A., Riddle, J., Desjardins-Langlais, Y., Baker, D.R. (2015) The effect of water on the sulfur concentration at sulfide saturation (SCSS) in natural melts. *Geochimica et Cosmochimica Acta* 160, 100–116. https://doi.org/10.1016/j.gca.2015.03.022

Gale, A., Dalton, C.A., Langmuir, C.H., Su, Y., Schilling, J.-G. (2013) The mean composition of ocean ridge basalts. *Geochemistry Geophysics Geosystems* 14, 489–518. https://doi.org/10.1029/2012GC004334

Jugo, P.J., Luth, R.W., Richards, J.P. (2005) An experimental study of the sulfur content in basaltic melts saturated with immiscible sulfide or sulfate liquids at 1300°C and 1 GPa. *Journal of Petrology* 46, 783–798. https://doi.org/10.1093/petrology/egh097

Kiseeva, E.S., Wood, B.J. (2013) A simple model for chalcophile element partitioning between sulphide and silicate liquids with geochemical applications. *Earth and Planetary Science Letters* 383, 68–81. https://doi.org/10.1016/j.epsl.2013.09.034

Kiseeva, E.S., Wood, B.J. (2015) The effects of composition and temperature on chalcophile and lithophile element partitioning into magmatic sulphides. *Earth and Planetary Science Letters* 424, 280–294. https://doi.org/10.1016/j.epsl.2015.05.012

Lord, O.T., Wann, E.T.H., Hunt, S.A., Walker, A.M., Santangeli, J., Walter, M.J., Dobson, D.P., Wood, I.G., Vocadlo, L., Morard, G., Mezouar, M. (2014) The NiSi melting curve to 70 GPa. *Physics of the Earth and Planetary Interiors* 233, 13–23. https://doi.org/10.1016/j.pepi.2014.05.005

Mahan, B., Siebert, J., Blanchard, I., Badro, J., Kubik, E., Sossi, P., Moynier, F. (2018) Investigating Earth's formation history through copper and sulfur metal-silicate partitioning during core-mantle differentiation. *Journal of Geophysical Research: Solid Earth* 123, 8349–8363. https://doi.org/10.1029/2018JB015991

O'Neil, H.St.C., Mavrogenes J.A. (2002) The sulfide capacity and the sulfur content at sulfide saturation of silicate melts at 1400°C and 1 bar. *Journal of Petrology* 43,1049–1087. https://doi.org/10.1093/petrology/43.6.1049

Palme, H., O'Neill, H.St.C (2014) 3.1 - Cosmochemical estimates of mantle composition. In: Holland, H.D., Turekian, K.K. (Eds.) *Planets, Asteroids, Comets and The Solar System, Treatise of Geochemistry (Second Edition).* Elsevier, Oxford, 1–39. https://doi.org/10.1016/B978-0-08-095975-7.00201-1

Peach, C.L., Mathez, E.A. (1993) Sulfide melt-silicate melt distribution coefficients for nickel and iron and implications for the distribution of other chalcophile elements. *Geochimica et Cosmochimica Acta* 57, 3013–3021.

Rubie, D.C., Jacobson, S.A., Morbidelli, A., O'Brien, D.P., Young, E.D., de Vries, J., Nimmo, F., Palme, H., Frost, D.J. (2015) Accretion and differentiation of the terrestrial planets with implications for the compositions of early-formed Solar System bodies and accretion of water. *Icarus* 248, 89–108. https://doi.org/10.1016/j.icarus.2014.10.015

Siebert, J., Badro, J., Antonangeli, D., Ryerson, F.J. (2012) Metal-silicate partitioning of Ni and Co in a deep magma ocean. *Earth and Planetary Science Letters* 321, 189–197. https://doi.org/10.1016/j.epsl.2012.01.013

Smythe, D.J., Wood, B.J., Kiseeva, E.S. (2017) The S content of silicate melts at sulfide saturation: New experiments and a model incorporating the effects of sulfide composition. *American Mineralogist* 102, 795–803. https://doi.org/10.2138/am-2017-5800CCBY

Steenstra, E.S., Seegers, A.X., Eising, J., Tomassen, B.G.J., Webers, F.P.F., Berndt, J., Klemme, S., Matveev, S., van Westrenen, W. (2018) Evidence for a sulfur undersaturated lunar interior from the solubility of sulfur in lunar melts and sulfide-silicate partitioning of siderophile elements. *Geochimica et Cosmochimica Acta* 231, 130–156. https://doi.org/10.1016/j.gca.2018.04.008

Steenstra, E.S., Berndt, J., Klemme, S., Snape, J.F., Bullock, E.S., van Westrenen, W. (2020a) The fate of sulfur and chalcophile elements during crystallization of the lunar magma ocean. *Journal of Geophysical Research*: *Planets* 125, e2019JE006328. https://doi.org/10.1029/2019JE006328

Steenstra, E. S., Trautner, V. T., Berndt, J., Klemme, S., van Westrenen, W. (2020b) Trace element partitioning between sulfides, metals and silicate melts at highly reduced conditions: insights into the depletion of volatile elements during core formation in

reduced bodies. *Icarus* 335, 113408. https://doi.org/10.1016/j.icarus.2019.113408

Suer, T.-A., Siebert, J., Remusat, L., Menguy, N., Fiquet, G. (2017) A sulfur-poor terrestrial core inferred from metal-silicate partitioning experiments. *Earth and Planetary Science Letters* 469, 84–97. https://doi.org/10.1016/j.epsl.2017.04.016

Tagawa, S., Sakamoto, N., Hirose, K., Yokoo, S., Hernlund, J., Ohishi, Y., Yurimoto, H. (2021) Experimental evidence for hydrogen incorporation into Earth's core. *Nature Communications* 12, 2588. https://doi.org/10.1038/s41467-021-22035-0

Wade, J., Wood, B.J. (2012) Metal-silicate partitioning experiments in the diamond anvil cell: A comment on potential analytical errors. *Physics of the Earth and Planetary Interiors* 192–193, 54–58. https://doi.org/10.1016/j.pepi.2011.12.002

Walter, M.J., Koga, K.T. (2004) The effect of chromatic dispersion on temperature measurement in the laser-heated diamond anvil cell. *Physics of the Earth and Planetary Interiors* 143–144, 541–558. https://doi.org/10.1016/j.pepi.2003.09.019

Walter, M.J., Thomson, A.R., Wang, W., Lord, O.T., Ross, J., McMahon, S.C., Baron, M.A., Melekhova, E., Kleppe, A.K., Kohn, S.C. (2015) The stability of hydrous silicates in Earth's lower mantle: Experimental constraints from the systems MgO-SiO_2-H_2O and MgO-Al_2O_3-SiO_2-H_2O. *Chemical Geology* 418, 16-29. https://doi.org/10.1016/j.chemgeo.2015.05.001

Wykes, J.L., O'Neill, H.St.C., Mavrogenes, J.A. (2015) The effect of FeO on the sulfur content at sulfide saturation (SCSS) and the selenium content at selenide saturation of silicate melts. *Journal of Petrology* 56, 1407–1424. https://doi.org/10.1093/petrology/egv041

Zhang, Y., Ni, H., Chen, Y. (2010) Diffusion data in silicate melts. *Reviews in Mineralogy and Geochemistry* 72, 311–408. https://doi.org/10.2138/rmg.2010.72.8